Journal of Oceanography, Vol. 57, pp. 549 to 563, 2001

Low Salinity, Cool-Core Cyclonic Eddy Detected Northwest of Luzon during the South China Sea Monsoon Experiment (SCSMEX) in July 1998

PETER C. CHU* and CHENWU FAN

Department of Oceanography, Naval Postgraduate School, Monterey, California 93943, U.S.A.

(Received 29 August 2000; in revised form 26 March 2001; accepted 26 March 2001)

To detect eddies, intensive surveys of the northeast South China Sea (SCS) (114°30′–121°30′ E, 17°–22°N) were conducted in July 1998 during the international SCS Monsoon Experiment (SCSMEX), the U.S. Navy using Airborne Expendable Bathythermograph and Conductivity-Temperature-Depth sensors (AXBT/AXCTD), and the Chinese Academy of Sciences using Acoustic Doppler Current Profilers (ADCP). The hydrographic survey included 307 AXBT and 9 AXCTD stations, distributed uniformly throughout the survey area. The ADCP survey had two sections. The velocity field inverted from the AXBT/AXCTD data and analyzed from the ADCP data confirm the existence of a low salinity, cool-core cyclonic eddy located northwest of Luzon Island (i.e., the Northwest Luzon Eddy). The radius of this eddy is approximately 150 km. The horizontal temperature gradient of the eddy increases with depth from the surface to 100 m and then decreases with depth below 100 m. The cool core was evident from the surface to 300 m depth, being 1°–2°C cooler inside the eddy than outside. The tangential velocity of the eddy is around 30–40 cm/s above 50 m and decreases with depth. At 300 m depth, it becomes less than 5 cm/s.

Keywords:
· Mesoscale eddies,
· South China Sea Monsoon Experiment (SCSMEX),
· P-vector method,
· airborne expendable bathythermograph (AXBT),
· airborne expendable CTD (AXCTD).

1. Introduction

The South China Sea (SCS) has a bottom topography (Fig. 1) that makes it a unique, semi-enclosed ocean basin that is temporally forced by a pronounced monsoon wind. Extended continental shelves (less than 100 m deep) exist along the north boundary and across the southwest portion of the basin, while steep slopes with almost no shelf are found along the eastern boundary. The deepest water is confined to an oblate bowl oriented SW-NE, centered around 13°N. The maximum depth is around 4500 m. The main connection between the SCS and the Pacific Ocean is via the Luzon Strait, which is very wide and has a sill depth of approximately 2400 m. Analyzing historical hydrographic data over a wide region of the northern SCS, Shaw (1989, 1991) found an evident intrusion current from the Philippine Sea over a wide region of the northern SCS in late autumn and winter.

Many studies have shown that the SCS has a multi-eddy structure. A survey by Wyrtki (1961) revealed complex temporal and spatial features of the surface currents in both the SCS and the surrounding waters. The general circulation of the SCS is predominantly cyclonic in winter and anticyclonic in summer. Reports from the South China Sea Institute of Oceanology (SCSIO) (1985) indicate that a warm-core eddy appears in summer and winter in the central SCS, but in summer it is closer to Vietnam at the surface. Soong *et al*. (1995) detected a cool-core eddy in the central SCS from December 29, 1993, to January 5, 1994, from an analysis of TOPEX/POSEIDON data. Chu *et al*. (1997a) and Chu and Chang (1997) identified the existence of a central SCS surface warm-core eddy in mid-May from a historical data set: the U.S. Navy's Master Observational Oceanographic Data Set (MOODS). From their composite analysis of the U.S. National Centers for Environmental Prediction (NCEP) monthly sea surface temperature (SST) fields (1982–1994), Chu *et al*. (1997b) found that during the spring-to-summer monsoon transition (March–May) a warm anomaly (greater than 1.8°C) is formed in the central SCS at 112°–119°30′ E, 15°–19°30′ N. From an extensive airborne expendable bathythermograph (AXBT) survey conducted in May 1995 and historical salinity data, Chu *et al*. (1998a) identified six eddies of the SCS (Fig. 2) using the P-vector inverse method (Chu, 1995, 2000; Chu *et*

* Corresponding author. E-mail: chu@nps.navy.mil

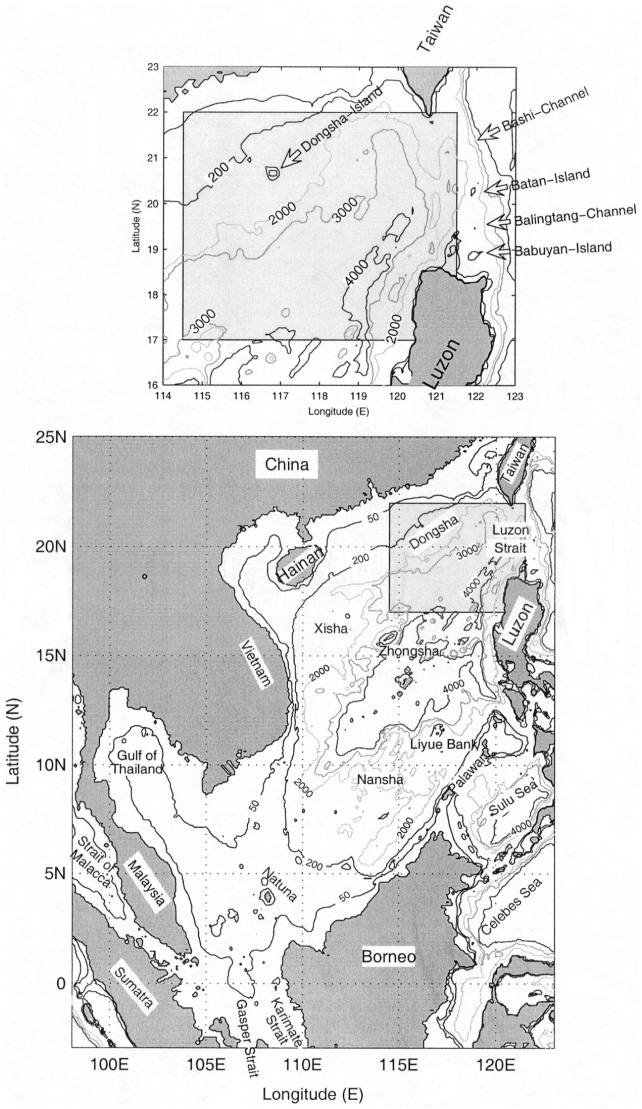

Fig. 1. Geography and isobaths showing the bottom topography of the South China Sea. The shaded box shows the survey area containing 307 AXBT and 9 AXCTD stations.

al., 1998b; Chu and Li, 2000): dual warm-core anticyclonic eddies in the central SCS and four surrounding cool-core cyclonic eddies located northwest of Luzon Island (i.e., NWL cold-core eddy), southeast of the Hainan Island, South Vietnamese coast, and Liyue Bank. In the upper layer the tangential velocity of the dual central SCS anticyclonic warm-core eddies is around 30–40 cm/s and that of the four cyclonic cool-core eddies varies from 10 cm/s to 40 cm/s. The tangential velocity of all the eddies decreased with depth, becoming less than 5 cm/s for all the eddies at 300 m depth. Furthermore, several numerical models (Li *et al*., 1992; Chao *et al*., 1996; Chu *et al*., 1999a, 1999b, 1999c, 2000; Wu *et al*., 1999) also simulated the existence of the multi-eddy structure in the SCS. Among these eddies, an eddy northwest of Luzon Island (hereafter referred to as the NWL eddy) is of interest because its location may affect the Kuroshio water entering the SCS.

The Kuroshio intrusion into the SCS through the Luzon Strait is an important process, influencing the hydrographic feature and circulation pattern in the north SCS (Nitani, 1970; Shaw, 1989, 1991; Chao *et al*., 1996; Li *et al*., 1998; Chu *et al*., 1999a, b). Two regimes (bifurcation and loop) of the northeast SCS (116°–120°E, 18°–23°N) circulation can be identified, based on the characteristics of the major eddy (i.e., the NWL eddy) in the area. If the NWL eddy is cyclonic (Qiu *et al*., 1985; Chu *et al*., 1998a), the northeast SCS circulation adopts the bifurcation pattern: the Kuroshio water is intruded into the SCS through the whole Luzon Strait and bifurcated into northward and northwestward branches before impinging the eddy. The northwestward branch was circulating around the cyclonic eddy (Fig. 3(a)). If the NWL eddy is anticyclonic (Li *et al*., 1998), the northeast SCS circulation adopts the loop pattern (Metzger and Hurlburt, 1996). The Kuroshio water is intruded into the SCS through the southern Luzon Strait. It loops around the anticyclone, exits the SCS through the northern Luzon Strait, and rejoins the Kuroshio current (Fig. 3(b)).

The NWL eddy was claimed to be either cold-core cyclonic or warm-core anticyclonic, based on the relative geostrophic velocity field calculated from hydrographic data. For example, Nitani (1970) used limited data to identify this eddy as cold-core cyclonic, occurring in the summer. Xu *et al*. (1982) used historical (1921–1970) hydrographic data to identify this eddy as cold-core cyclonic, occurring in the winter. Zhou *et al*. (1995) confirmed the occurrence of the NWL cold-core cyclonic eddy in both winter and summer, using climatological monthly mean temperature and salinity data. Recently, Li *et al*. (1998) analyzed the hydrographic data collected during a major expedition of the Northeastern SCS Circulation Cooperative Study in August–September 1994 and identified the NML eddy as warm-core anticyclonic. All of these observational studies are reliant on the level assumed for no-motion. For example, Xu *et al*. (1982) and Li *et al*. (1998) assumed 1200 db and 1000 db as the level of no-motion, respectively. To remove the effect of the assumption about the level of no-motion, Chu *et al*. (1998a) used the P-vector inverse method (Chu, 1995) to identify the NWL cold-core cyclonic eddy from an extensive AXBT survey conducted in May 1995 and historical salinity data.

One objective of the international SCS Monsoon Experiment (SCSMEX) is to detect the SCS eddy features. During the intensive observational period of the SCSMEX in July 1998, the U.S. Naval Oceanographic

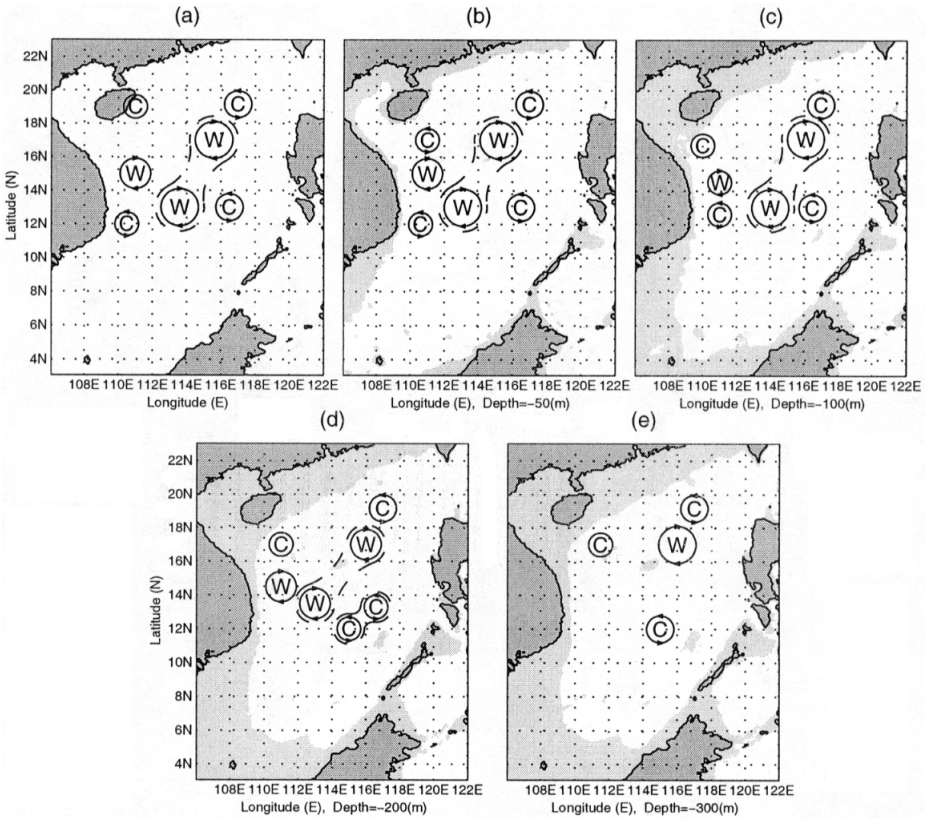

Fig. 2. A multi-eddy structure of the SCS in May 1995 detected by the AXBT measurements (after Chu *et al.*, 1998a).

Office conducted an intensive airborne expendable hydrographic survey of the northeast South China Sea (SCS) on July 8–26, 1998. The Chinese Academy of Sciences conducted the ADCP measurements aboard R/V Shiyan3. The airborne hydrographic survey includes 307 AXBT stations and 9 airborne expendable conductivity-temperature-depth (AXCTD) stations, uniformly distributed in the region (114°30′–121°30′ E, 17°–22°N), shown in Fig. 1 as the shaded box. Due to the Navy's regulations, we are unable to present the T, S station distribution. The maximum depth of the observations is 400 m. This data set provides something close to a snapshot of the temperature and salinity in the upper ocean in the northeast SCS in July 1998. With synoptic T, S data, we may obtain a more accurate estimation of the NWL eddy using the P-vector inverse method.

The outline of this paper is as follows. A description of the AXBT/AXCTD and ADCP measurements is given in Section 2. Data analysis is given in Section 3. The synoptic three-dimensional thermohaline structure and the inverted velocity field are discussed in Sections 4–6. The energy budget of the NWL eddy and surrounding areas is given in Section 7. In Section 8 we present our conclusions.

2. Observations

AXBTs/AXCTDs were deployed over a period of July 8–26, 1998. The majority of AXBTs/AXCTDs were nominally capable of reaching a depth of 400 m. The vertical resolution of the measurements is 1 m.

We computed the *in-situ* density with 1 m vertical resolution from the 9 AXCTD stations. The horizontal averages of 316 temperature stations, 9 salinity stations, and 9 *in-situ* density profiles at each depth lead to the vertical mean profiles of temperature, $\overline{T}(z)$, salinity, $\overline{S}(z)$, and density, $\overline{\rho}(z)$. From the mean density profile, we computed the buoyancy frequency,

$$N = \sqrt{-\frac{g}{\rho_0}\frac{d\overline{\rho}(z)}{dz}}$$

where ρ_0 is the characteristic value of the density field. In this study we use the vertical mean of $\overline{\rho}(z)$ to represent ρ_0.

The mean temperature profile shows a very shallow mixed layer of depth less than 20 m (Fig. 4(a)). Below the mixed layer, the mean temperature reduces rapidly with depth from 29.5°C at the base of the mixed layer

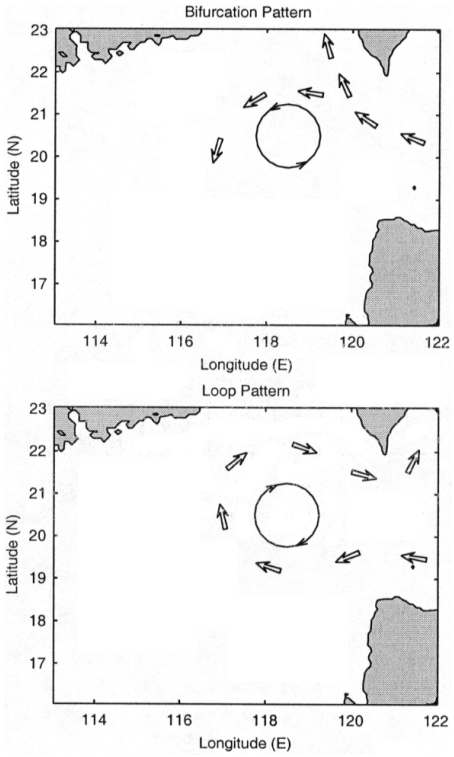

Fig. 3. Two regimes of the northeast SCS circulation: (a) bifurcation pattern, and (b) loop pattern.

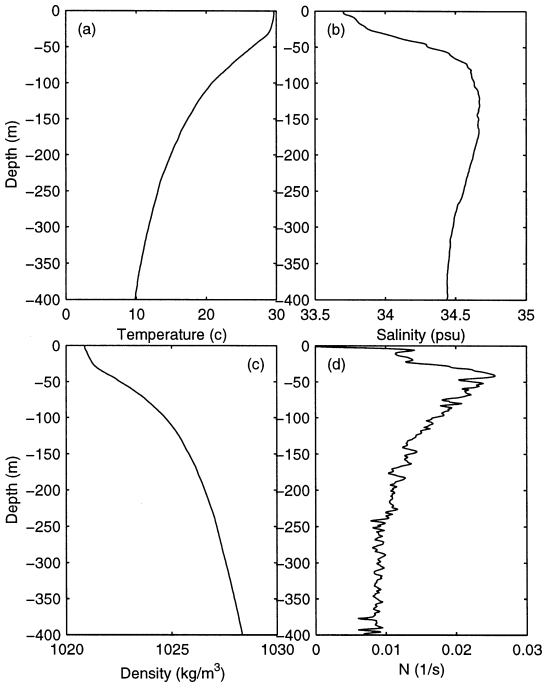

Fig. 4. Mean vertical profiles of (a) temperature, (b) salinity, (c) density, and (d) buoyancy frequency.

(20 m) to 20°C at 100 m depth, and then reduces slowly with depth from 20°C at 100 m depth to 10°C at 400 m depth. The mean salinity profile (Fig. 4(b)) shows the existence of salinity maxima (~34.63 ppt) located at 125–175 m depth and of salinity minima (~34.43 ppt) located at 400 m depth. The mean density profile (Fig. 4(c)) shows that the vertical variability of $\overline{\rho}(z)$ follows the vertical variability of $\overline{T}(z)$. The buoyancy frequency (Fig. 4(d)) increases with depth from 0 at the surface to a maximum value (~0.026 s^{-1}) at 45 m depth and then tends to reduce with depth to a minimum value (~0.007 s^{-1}) at 400 m depth.

The current observations were made aboard R/V Shiyan3 on July 16–21, 1998. That vessel was equipped with an ADCP and a global position system (GPS) receiver. This system measured currents underway from depths of about 10 to 250 m in 4 m depth bins. Five minute averages were recorded.

3. Data Analysis

3.1 Temperature

The AXBT/AXCTD observations (316 stations) were mapped on (1/4)° × (1/4)° grids at each depth using a two-scale optimal interpolation (OI) scheme (Gandin, 1965; Lozano *et al*., 1996). The large-scale OI was used to estimate the background mean with a decorrelation scale of 450 km. The mesoscale OI was used to map the observational anomaly from the background mean field into a regular grid with a spatial decorrelation scale of 75 km and a temporal decorrelation scale of 10 days. The spatial and temporal decorrelation scales associated with the mean field were estimated from the covariance matrix obtained from MOODS for the SCS (see Chu *et al*., 1997c). The large-scale mean was computed using the temperature and salinity profiles. The large-scale pattern for the surface (not shown) resembles the pattern previously estimated by Chu *et al*. (1997c). The decorrelation length scale for the fluctuations from the mean was estimated from the AXBT data. The results shown below are relatively insensitive to the length scale in the range of 60–90 km. The decorrelation time scale was selected to ensure synopticity. The SST horizontal scales seem somewhat larger than temperatures in the seasonal thermocline. In this study, we choose horizontal scales to be uniform in the vertical for convenience and for lack of sufficient data to discriminate these differences properly. We use T^* to represent the gridded 3-D temperature field.

3.2 Salinity

The salinity observations S from AXCTD were uniformly distributed in the area, but very sparse (9 stations).

We use the same OI scheme as described in the previous section (Lozano *et al.*, 1996) to blend the AXCTD salinity data with the Navy's public domain Global Digital Environmental Model (GDEM) climatological monthly mean (July) salinity data set (Teague *et al.*, 1990). The blended salinity field (S^*) were also on (1/4)° × (1/4)° grids.

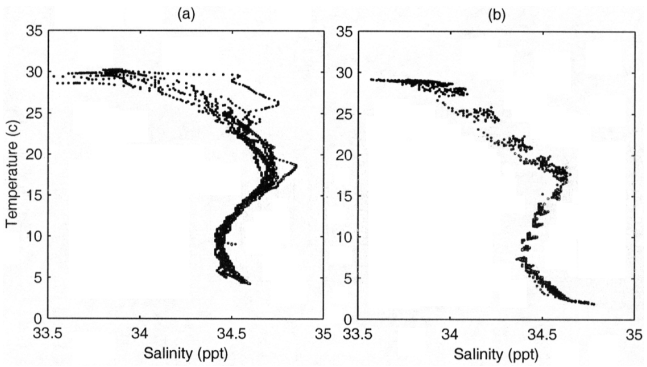

Fig. 5. (a) *T-S* diagram constructed from the AXCTD data, and (b) T^*-S^* diagram constructed from the interpolated data.

3.3 T-S and T-S* diagrams*

To validate this technique for the establishment of gridded temperature and salinity data, we plotted two *T-S* diagrams: One is the plot of nine *T*, *S* profiles from AXCTD measurements in July 1998 (Fig. 5(a)) and the other is the plot of gridded data T^* and S^* (Fig. 5(b)). Both diagrams show the typical northeast SCS sea water depicted by Li *et al*. (1998): The salinity maxima are less than 34.7 ppt and the salinity minima are larger than 34.40 ppt. Comparison between the two shows that the *T-S* characteristics remain stable.

However, we should be aware of the shortcomings in using the (T^*, S^*) data for inverting the absolute geostrophic velocity field. If the temperature field is relatively homogeneous in space, the density gradient depends mostly on the salinity gradient. Under that circumstance, the use of the blended salinity values may introduce large errors in the inversion.

4. Temperature Field

4.1 Horizontal structures

Figure 6 shows the horizontal depictions of temperature at nine different depths from the surface to 400 m

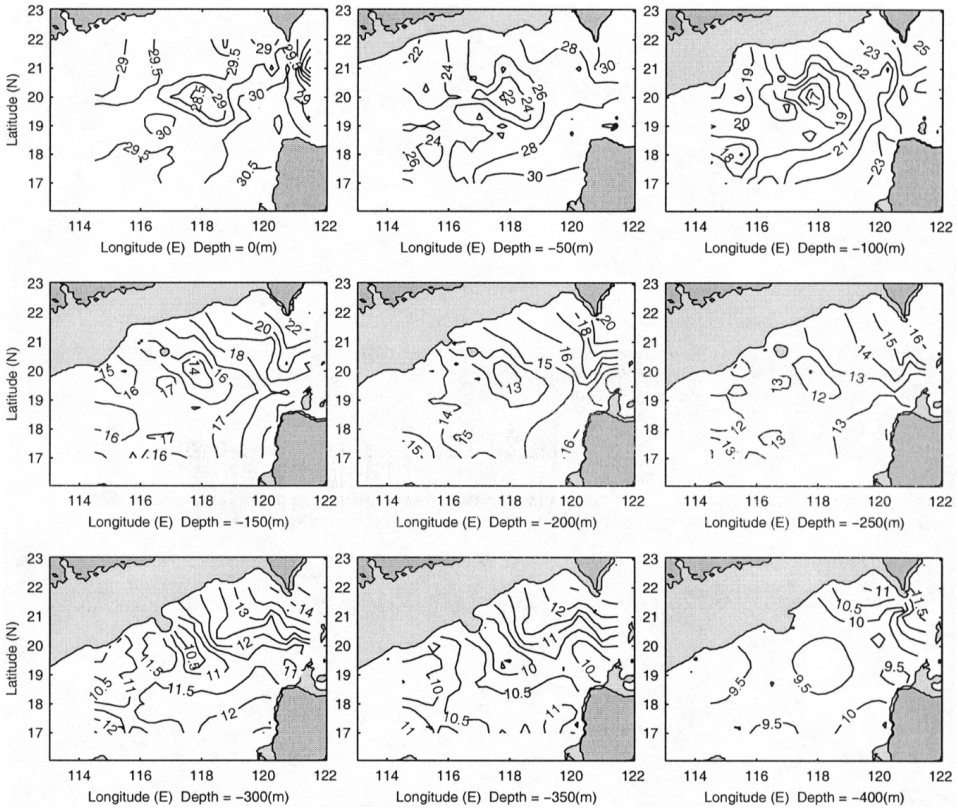

Fig. 6. Horizontal temperature fields at 9 different depths from the surface to 400 m at 50 m intervals. Cooler water is situated northwest of Luzon Island (116°–119°E, 19°–21.5°N), surrounded by warmer water.

Table 1. Locations, typical temperatures, salinities, and tangential velocities of NWL low salinity cool-core cyclonic eddy.

Depth (m)	Location	Temperature (°C)	Salinity (ppt)	Maximum tangential velocity (cm/s)
0	19°–21°N; 116.5°–119°E	28.5	33.60	50
50	18.8°–21.5°N; 116.5°–119°E	22	34.40	45
100	18.8°–21.5°N; 116.75°–119°E	17		20
150	19°–20.8°N; 116.5°–119°E	14	34.64	12
200	18.5°–21°N; 117°–119°E	13	34.56	6
250	19°–21°N; 116.5°–119°E	12	34.50	6
300	18.8°–20.8°N; 117°–119°E	10.5	34.46–34.47	5

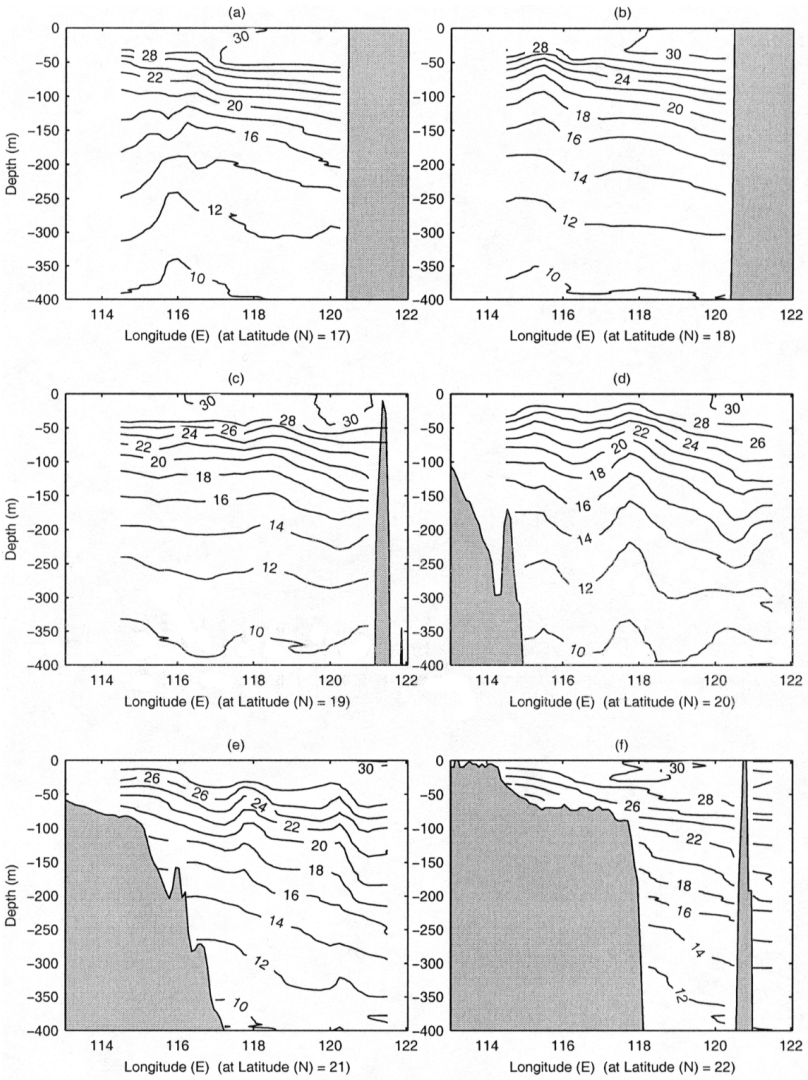

Fig. 7. Temperature distribution at several zonal cross-sections: (a) 17°N, (b) 18°N, (c) 19°N, (d) 20°N, (e) 21°N, and (f) 22°N.

depth, at 50 m intervals. The reader can see a cool-core ring situated northwest of Luzon Island (116°–119°E, 19°–21.5°N) surrounded by warmer water. The horizontal temperature gradient across the eddy increases with depth from the surface to 100 m and then decreases with depth below 100 m. The cool core was evident from the surface to 300 m depth, being 1°–2°C cooler inside than outside the eddy. The location and thermal features of the NWL cool-core eddy are listed in Table 1.

4.2 Vertical structures

4.2.1 Zonal cross-sections

Six zonal cross-sections of temperature, from 17° to 22°N (Fig. 7), show the vertical layered structure (mixed layer, thermocline, and layer below the thermocline). A cool core can be identified by the uplifting (ridge) of isotherms and a warm core can be identified from the downward bending (trough) of the isotherms.

The mixed layer is not evident at the 22°N cross section but becomes evident as latitude decreases. From the 21° to 17° N cross sections, the mixed layer shallows toward the west. A shallow layer (<50 m depth) of warm water with temperature higher than 30°C occurs in the Luzon Strait (120°–120.7°E) at the 20°N cross-section. This warm water extends westward as the latitude decreases. At the 17°N cross-section, the warm water ($T >$ 30°C) reaches 117°E.

The cross-sections from the 21°N to 19°N clearly show the existence of the NWL cool core near 117.5° from the uplifting (ridge) of isotherms. Taking the 20°N cross-

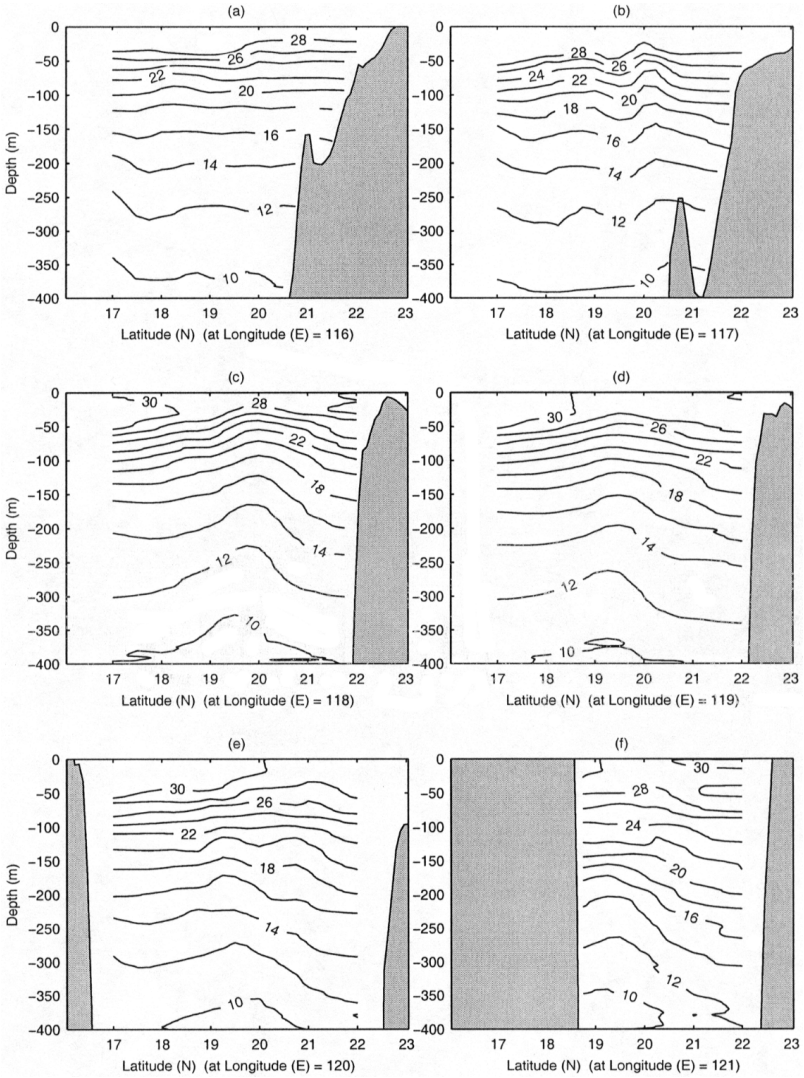

Fig. 8. Temperature distribution at several latitudinal cross sections: (a) 116°E, (b) 117°E, (c) 118°E, (d) 119°E, (e) 120°E, and (f) 121°E.

section as an example, the ridge is located at 117.8°E from the surface to the 400 m depth. The longitudinal span of the NWL cool eddy is around 300 km.

4.2.2 Meridional cross-sections

Six meridional cross-sections from 116° to 121°E of temperature (Fig. 8) show the same vertical layered structure (mixed layer, thermocline, and layer below the thermocline). The mixed layer shallows toward the north in the western cross-sections (115°–116.5°E). A shallow layer (<50 m depth) of warm water (T > 30°C) occurs in the southern part of the Luzon Strait (south of 20.3°N) at the 120°E cross-section. This warm water retreats toward the south as the longitude decreases. The warm water (T > 30°C) disappears at the 117°E cross-section.

The cross-sections from 117° to 119°N clearly show the existence of the NWL cool core near 18°–21°N from the uplifting (ridge) of isotherms. Taking the 118°E cross-section as an example, the ridge is located at 20°N from the surface to 400 m depth. The latitudinal span of the NWL cool eddy is around 300 km.

5. Salinity Field

5.1 Horizontal structures

Figure 9 shows the horizontal depictions of salinity at nine different depths from the surface to 400 m depth with 50 m interval. In them, we see low salinity centers associated with the NWL cool-core eddy at various depths: a low salinity center (S < 33.60 ppt) with the NWL cool core (T < 29°C) at the surface, a low salinity tongue (S < 34.64 ppt) with the NWL cool core (T < 14°C) at 150 m depth. The low salinity tongue retreats northwestward below 200 m depth.

5.2 Vertical structures

5.2.1 Zonal cross-sections

Six zonal cross sections of salinity, from 17° to 22°N (Fig. 10) show a strong northward uplifting of the halocline with 30–50 m depth north of 20°N and 40–75 m depth south of 20°N. The strength of the halocline decreases toward the south. The cross-sections of 17°N to

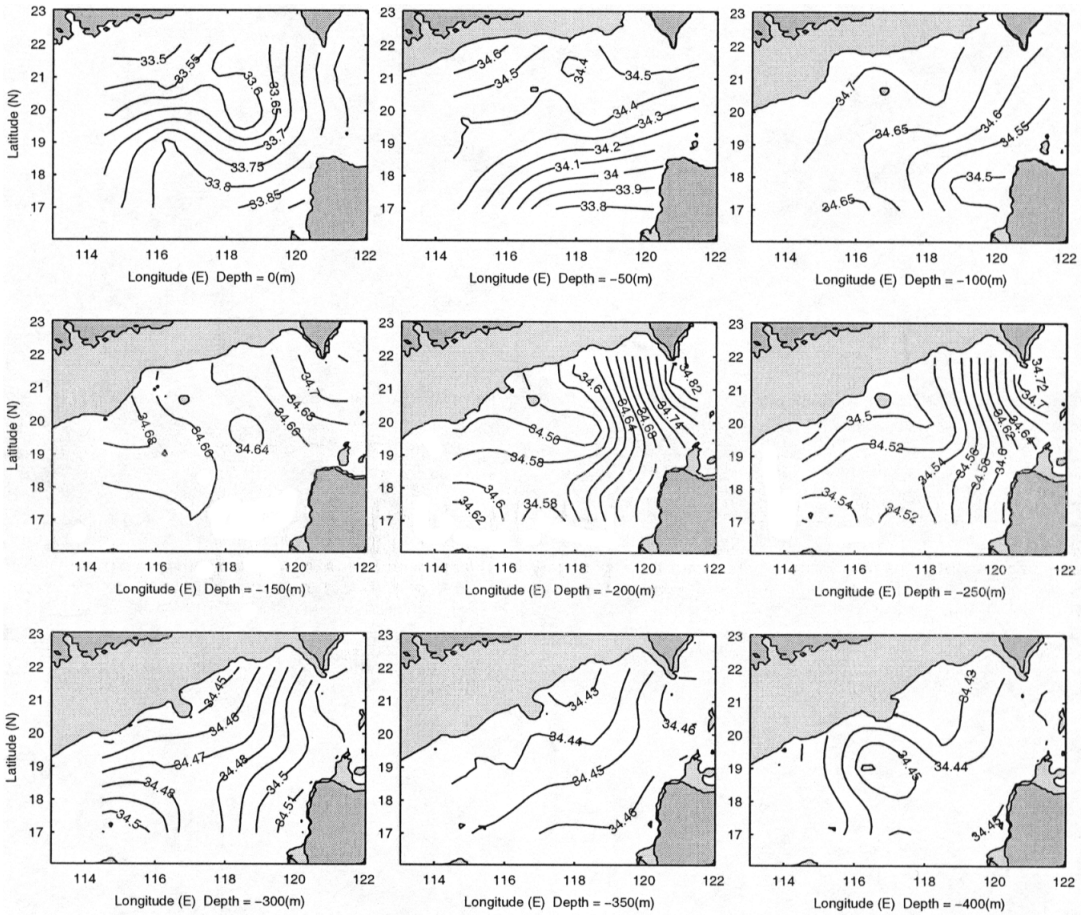

Fig. 9. Horizontal salinity fields at 9 different depths from the surface to 400 m at 50 m intervals. Fresher water is situated northwest of Luzon Island, surrounded by saltier water.

18°N show an evident westward uplifting of the halocline. Below the halocline, salinity maxima (>34.7 ppt) can be identified from all the cross-sections with shallow depths (100–150 m) west of 119°E and with deep ones (150–250 m) east of 119°E. A low-salinity core can be identified by the uplifting of the isohalines or by sandwiching between the two salinity maxima. Looking at the 20°N cross-section, the western salinity maximum occurs west of 119°E between 100 and 150 m depths, and the eastern salinity maximum occurs east of 120°E between 150 and 250 m depths. Between the two salinity maxima there is a low salinity area, co-located with the NWL cool-core eddy.

5.2.2 Meridional cross-sections

Six latitudinal cross-sections of salinity, from 115° to 121°E (Fig. 11) show the same features as Fig. 10, with a strong halocline occurring at all cross-sections. The halocline has an evident northward uplift, and eastward decrease. Below the halocline, two salinity maxima (north and south) can be identified from several cross-sections, with a salinity minimum in between. Looking at the 117°E cross-section, the southern salinity maximum (>34.7 ppt) occurs south of 18.2°N between 120 and 150 m depths, and the northern salinity maximum (>34.7 ppt) occurs north of 19.5°N between 75 and 125 m depths. Between the two salinity maxima, there is a low salinity area, co-located with the NWL cool-core eddy. Thus, the salinity is usually lower inside than outside the NWL cool-core eddy.

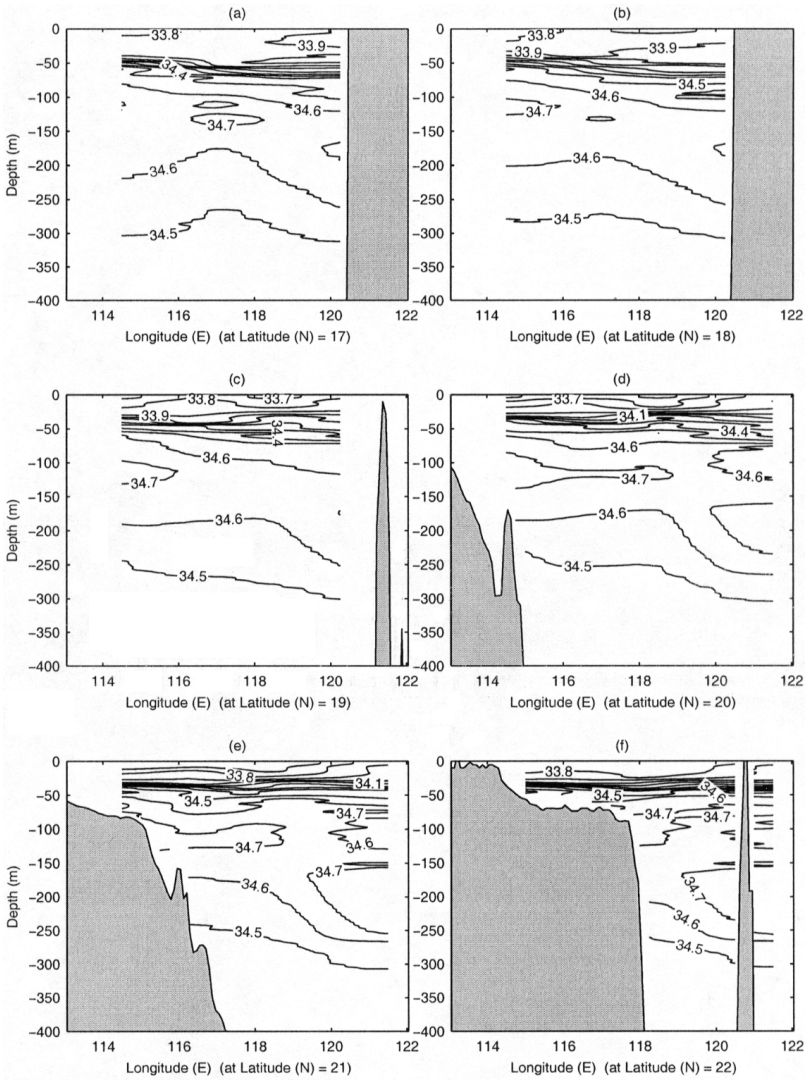

Fig. 10. Salinity distribution at several zonal cross-sections: (a) 17°N, (b) 18°N, (c) 19°N, (d) 20°N, (e) 21°N, and (f) 22°N.

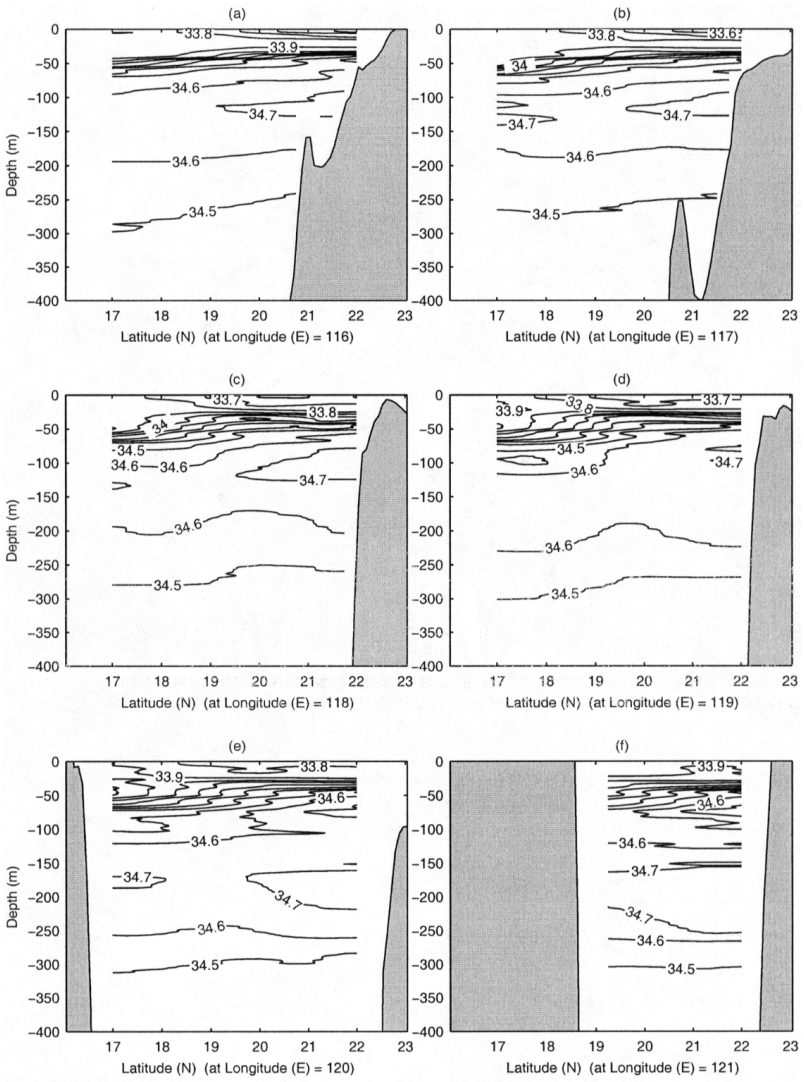

Fig. 11. Salinity distribution at several meridional cross-sections: (a) 116°E, (b) 117°E, (c) 118°E, (d) 119°E, (e) 120°E, and (f) 121°E.

6. NWL Eddy

The P-vector inverse method (Chu, 1995, 2000; Chu *et al*., 1998a, b; Chu and Li, 2000) was used to determine the velocity field from the temperature and salinity data. The optimization scheme proposed by Chu *et al*. (1998a) was also used to minimize errors in this study.

6.1 Horizontal velocity fields

The inverted velocity vectors near Luzon Strait (Fig. 12) clearly show a pattern of upper layer (above 200 m depth) evident Kuroshio intrusion and lower layer (below 200 m depth) weak SCS outflow. The upper layer flow pattern is quite similar to the bifurcation pattern depicted in Fig. 3(a). The upper layer intruded Kuroshio water bifurcates into northward and northwestward branches west of the Balingtang Channel (120°20′ E, 19°30′ N). The northwestward branch circulates around the cool-core area (116°–119°E, 19°–21.5°N) and forms a cyclonic eddy (i.e., upper part of the NWL baroclinic eddy). The maximum tangential velocity of the eddy decreases with depth from around 0.5 m s^{-1} at the surface to 0.06 m s^{-1} at 200 m depth. The radius of the eddy is around 150 km. There is a smaller and weaker anticyclonic eddy associated with the warm-core ring southwest of the NWL eddy.

Comparing Fig. 12 with Figs. 6 and 9, we find that the NWL cyclonic eddy is cooler and fresher than the surroundings. The location and kinetic features of the

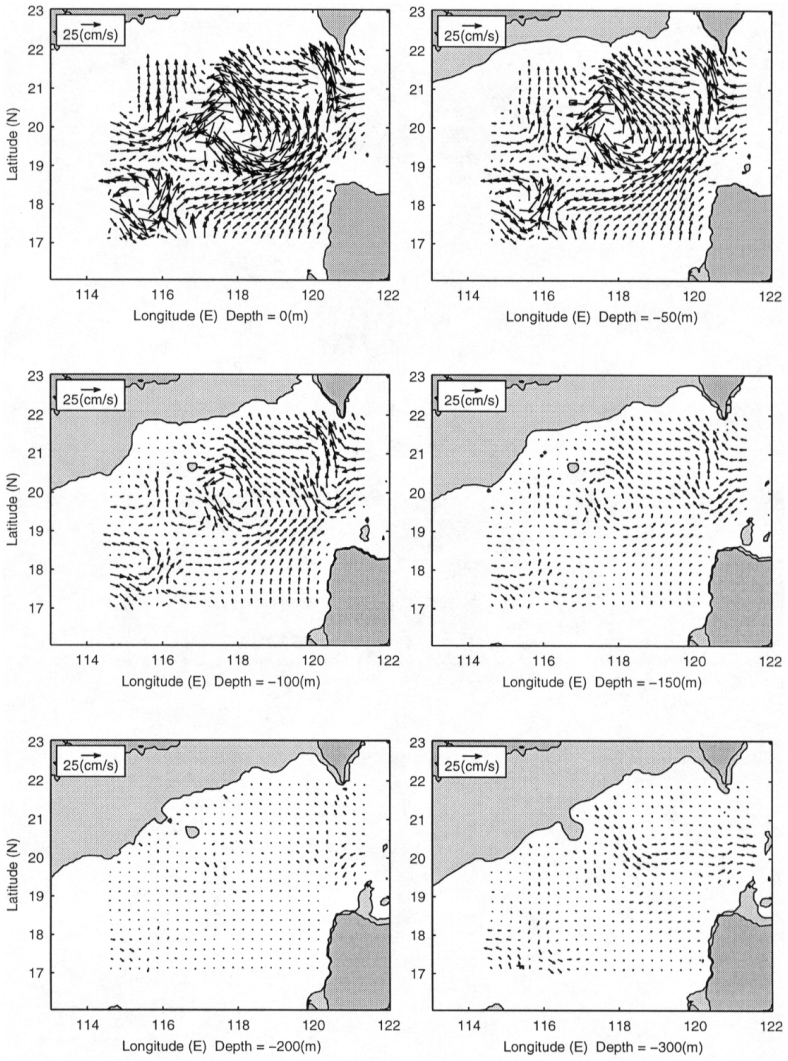

Fig. 12. Absolute velocity vectors at different depths: (a) 0 m, (b) 50 m, (c) 100 m, (d) 200 m, and (e) 300 m. The NWL baroclinic eddy is cyclonic in the upper layer from the surface to 200 m depth and anticyclonic in the lower layer below 200 m depth.

Table 2. Locations, typical temperatures, salinities, and tangential velocities of the NWL core-core eddy.

Depth (m)	Location	Temperature (°C)	Salinity (psu)	Type of rotation	Maximum tangential velocity (cm/s)
0	19°–21°N; 116.5°–119°E	28.5	33.60	Cyclonic	50
50	18.8°–21.5°N; 116.5°–119°E	22	34.40	Cyclonic	45
100	18.8°–21.5°N; 116.75°–119°E	17		Cyclonic	20
150	19°–20.8°N; 116.5°–119°E	14	34.64	Cyclonic	12
200	18.5°–21°N; 117°–119°E	13	34.56	Cyclonic	6
250	19°–21°N; 116.5°–119°E	12	34.50	Anticyclonic	8
300	18.8°–20.8°N; 117°–119°E	10.5	34.46–34.47	Anticyclonic	12
350	18.8°–20.8°N; 117°–119°E	10	34.44–34.45	Anticyclonic	12
400	18.8°–20.8°N; 117°–119°E	9.5	34.45	Anticyclonic	15

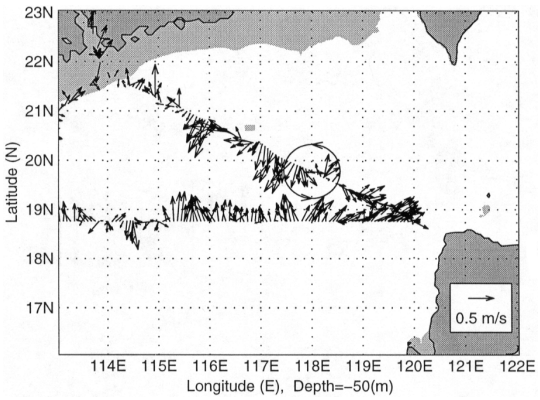

Fig. 13. ADCP velocity vectors (15 min averages) at 50 m depth measured during the SCSMEX on July 16–21, 1998 from R/V Shiyan3. Note the cyclonic circulation pattern centered 118°E, 19.5°N with the zonal span of around 300 km. The maximum velocity is 1 m s^{-1}.

NWL eddy at different depths are listed in Table 2. Several weak, small eddies were also found west and southwest of the NWL eddy.

The current vectors at 50 m as measured by the ADCP aboard R/V Shiyan3 are shown in Fig. 13. At this depth, a cyclonic eddy can be identified, centered at 118°E, 19.5°N and having a zonal span of around 300 km. The maximum velocity is 1 m s^{-1}, which is higher than the speed inverted from the hydrographic data. A strong convergence of current vectors occurs at around 20°N, 115.5°E in the ADCP data (total flow), but not in the inverted data (geostrophic flow). Such a discrepancy may suggest the importance of an ageostrophic component.

6.2 Zonal cross-sections of v component

Six zonal cross-sections, from 17°N to 22°N, of *v*-velocity show the vertical structure of the NWL eddy (Fig.

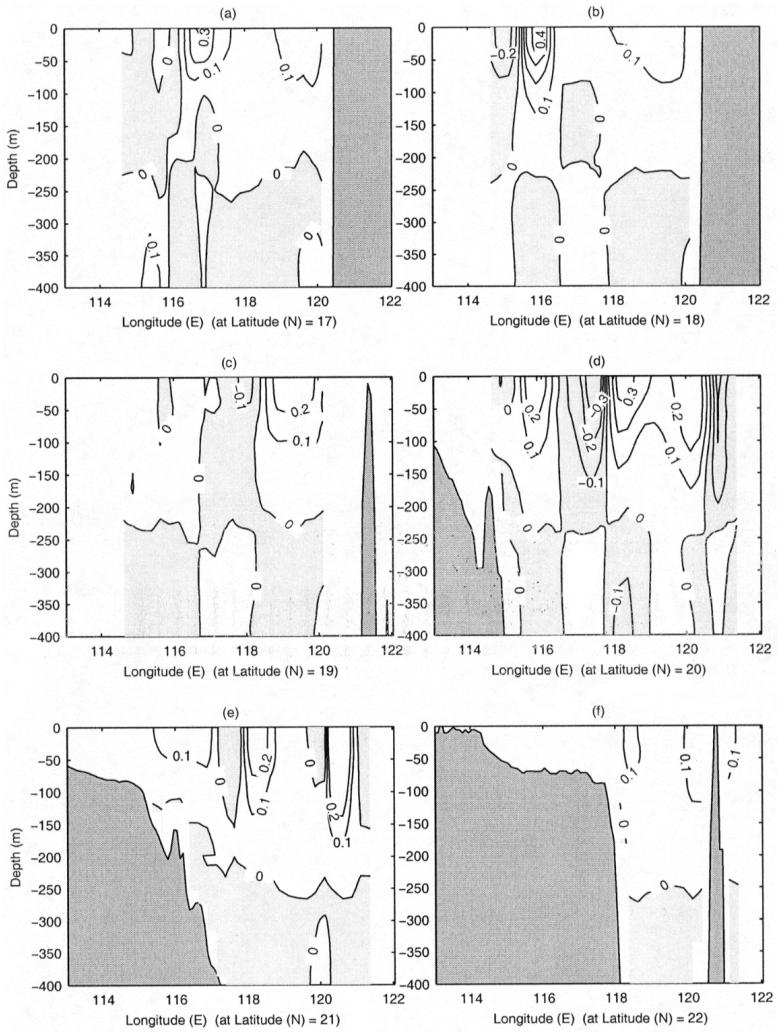

Fig. 14. Distribution of inverted velocity *v* component at several zonal cross sections: (a) 17°N, (b) 18°N, (c) 19°N, (d) 20°N, (e) 21°N, and (f) 22°N.

14). The positive values indicate a northward velocity, and the negative values refer to the southward velocity. Between 116°E and 119°E (the zonal span of the NWL eddy), the NWL baroclinic eddy can be identified by alternate positive and negative areas at the zonal cross-sections of 19°N, 20°N, and 21°N. At each zonal cross-section, we found a cyclonic rotation in the upper layer (surface to 200 m depth) from a neighboring eastern positive/western negative pattern and an anticyclonic rotation in the lower layer (below the 200 m depth) from a neighboring eastern negative/western positive pattern. The upper layer cyclonic rotation was quite strong, with the maximum *v*-velocity higher than 0.3 ms^{-1}. The lower layer anticyclonic rotation was much weaker, with the maximum *v*-velocity around 0.1 ms^{-1}.

7. Energy Budget of the NWL Eddy

7.1 Mean kinetic energy

We computed the horizontal mean kinetic energy per unit mass at each depth,

$$\bar{u}(z) = \frac{1}{M}\sum_i\sum_j u(x_i, y_j, z), \quad \bar{v}(z) = \frac{1}{M}\sum_i\sum_j v(x_i, y_j, z) \quad (1)$$

where M is the total number of horizontal grid points. The mean kinetic energy $\bar{K}$ is defined by

$$\bar{K}(z) = \frac{1}{2}\left[\bar{u}(z)^2 + \bar{v}(z)^2\right]. \quad (2)$$

Figure 15 shows the vertical profile of the mean kinetic energy. The mean kinetic energy, $\bar{K}$, has a maximum value of 3.5×10^{-3} m^2/s^2 at the surface. It decreases with the depth from the surface maximum value to zero at 200 m depth. Between 200 and 250 m, the mean kinetic energy is very small (near zero). Below 250 m depth, the mean kinetic energy increases slightly with depth. This may imply that the mean circulation reversal occurs between 200 and 250 m.

7.2 Eddy kinetic energy

The eddy kinetic energy can be computed by

$$K' = \frac{1}{2}\left(u'^2 + v'^2\right) \quad (3)$$

where

$$u'(x_i, y_j, z) = u(x_i, y_j, z) - \bar{u}(z),$$
$$v'(x_i, y_j, z) = v(x_i, y_j, z) - \bar{v}(z).$$

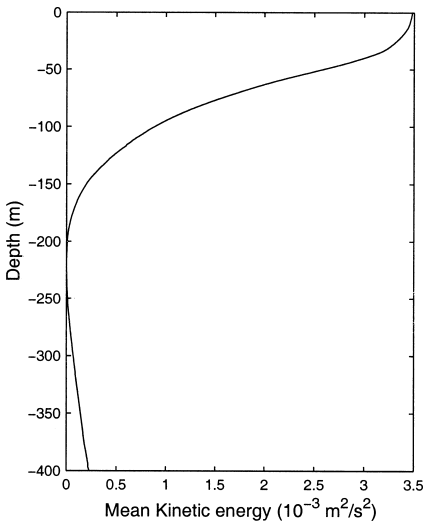

Fig. 15. Vertical dependence of the mean kinetic energy per unit mass, $\bar{K}$ (in: $10^{-3}m^2s^{-2}$).

The horizontal distributions of K' at different depths (Fig. 16) clearly show the isolated eddy structure such as the NWL eddy in the middle of the region (18°–22°N, 116.5°–119°E). Its eddy kinetic energy has a maximum value (0.19 m^2/s^2) at the surface, and decreases with depth to 0.8×10^{-2} m^2/s^2 at 300 m depth. The maximum eddy kinetic energy is 1–2 orders of magnitude larger than the mean kinetic energy.

8. Conclusions

(1) Objective analysis of the AXBT/AXCTD data allowed us to identify the occurrence of a cool-core, low salinity eddy northwest of Luzon Island (116°–119°E, 19°–21.5°N) during July 8–26, 1998. This cool-core, low salinity eddy was quite isolated, with a radius of around 150 km. The cool, low salinity core was evident at all levels, being 1°–2°C cooler and 0.02–0.1 ppt lower salinity inside the eddy than outside it.

(2) The detected NWL cool-core eddy is cyclonic. The inverted upper layer circulation in the northeast SCS has a bifurcation pattern. The intruded Kuroshio water bifurcates into northward and northwestward branches near the Balingtang Channel (120°20′ E, 19°30′ N). The northwestward branch circulates around the cool-core area (116°–119°E, 19°–21.5°N) and forms a cyclonic eddy. The maximum tangential velocity of the eddy decreases with depth from around 0.5 m s^{-1} at the surface to 0.06 m s^{-1} at 200 m depth. The radius of the eddy is around 150 km. This cyclonic eddy was also observed from the ADCP data.

(3) The AXCTD data show the existence of an evident halocline between 30–50 m depth north of 20°N and 40–75 m depth south of 20°N. The strength of the

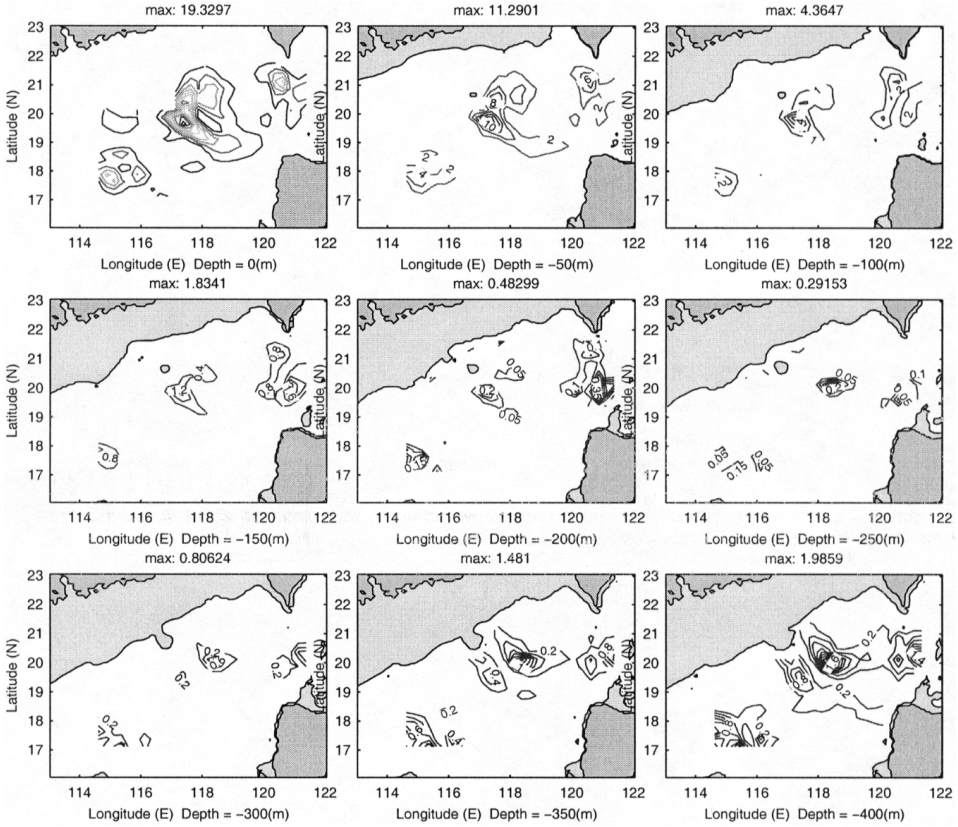

Fig. 16. Horizontal distribution of eddy kinetic energy per unit mass, K' (in $10^{-2}m^2s^{-2}$), at nine different depths.

halocline decreases toward the south. Below the halocline, salinity maxima (>34.7 ppt) can be identified with shallow depths (100–150 m) west of 119°E and with deep ones (150–250 m) east of 119°E. The low salinity cool-core inside the NWL eddy can be identified by the uplifting of the isohalines or by the sandwiching between the two salinity maxima.

(4) The mean kinetic energy per unit mass in the northeast SCS had a maximum value of 3.5×10^{-3} m^2/s^2 at the surface. It decreased with depth from the surface maximum value to zero at 200 m depth. Between 200 and 250 m, the mean kinetic energy was very small (near zero). Below 250 m depth, the mean kinetic energy increased slightly with depth.

(5) The eddy kinetic energy per unit mass indicated the isolated eddy structure. The eddy kinetic energy had a maximum value (0.19 m^2/s^2) at the surface, decreasing with depth to 0.8×10^{-2} m^2/s^2 at 300 m depth. The maximum eddy kinetic energy was 1–2 orders of magnitude larger than the mean kinetic energy.

Acknowledgements

Many thanks are due to the Naval Oceanographic Office and the SCSMEX Data Center for providing the AXBT/AXCTD and the ADCP data, respectively. This work was funded by the Naval Oceanographic Office, the Office of Naval Research, and the Naval Postgraduate School.

References

Chao, S. Y., P. T. Shaw and J. Wang (1996): Deep water ventilation in the South China Sea. *Deep-Sea Res.*, **43**, 445–466.

Chu, P. C. (1995): P vector method for determining absolute velocity from hydrographic data. *Mar. Technol. Soc. J.*, **29**(3), 3–14.

Chu, P. C. (2000): P-vector spirals and determination of absolute velocities. *J. Oceanogr.*, **56**, 591–599.

Chu, P. C. and C. P. Chang (1997): South China Sea warm pool in boreal spring. *Adv. Atmos. Sci.*, **14**, 195–206.

Chu, P. C. and R. F. Li (2000): South China Sea isopycnal surface circulations. *J. Phys. Oceanogr.*, **30**, 2,419–2,438.

Chu, P. C., H. C. Tseng, C. P. Chang and J. M. Chen (1997a): South China Sea warm pool detected in spring from the Navy's Master Oceanographic Observational Data Set (MOODS). *J. Geophys. Res.*, **102**, 15,761–15,771.

Chu, P. C., S. H. Lu and Y. C. Chen (1997b): Temporal and spatial variabilities of the South China Sea surface temperature anomaly. *J. Geophys. Res.*, **102**, 20,937–20,955.

Chu, P. C., S. K. Wells, S. D. Haeger, C. Szczechowski and M.

Carron (1997c): Temporal and spatial scales of the Yellow Sea thermal variability. *J. Geophys. Res*., **102**, 5,655–5,667.

Chu, P. C., C. W. Fan, C. J. Lozano and J. Kerling (1998a): An airborne expandable bathythermograph (AXBT) survey of the South China Sea, May 1995. *J. Geophys. Res*., **103**, 21,637–21,652.

Chu, P. C., C. W. Fan and W. J. Cai (1998b): P vector inverse method evaluated using the Modular Ocean Model (MOM). *J. Oceanogr*., **54**, 185–198.

Chu, P. C., N. L. Edmons and C. W. Fan (1999a): Dynamical mechanisms for the South China Sea seasonal circulation and thermohaline variabilities. *J. Phys. Oceanogr*., **29**, 2,971–2,989.

Chu, P. C., S. H. Lu and W. T. Liu (1999b): Uncertainty of the South China Sea prediction using NSCAT and NCEP winds during tropical storm Ernie 1996. *J. Geophys. Res*., **104**, 11,273–11,289.

Chu, P. C., S. H. Lu and Y. C. Chen (1999c): A coastal air-ocean coupled system (CAOCS) evaluated using an airborne expandable bathythermograph (AXBT) data set. *J. Oceanogr*., **55**, 543–558.

Chu, P. C., J. M. Veneziano and C. W. Fan (2000): Response of the South China Sea to tropical cyclone Ernie 1996. *J. Geophys. Res*., **105**, 13,991–14,009.

Gandin, L. S. (1965): *Objective Analysis of Meteorological Fields*. Israel Program for Scientific Translation, Jerusalem, 242 pp.

Li, L., W. D. Nowlin, Jr. and J. Su (1998): Anticyclonic rings from the Kuroshio in the South China Sea. *Deep-Sea Res. I*, **45**, 1,469–1,482.

Li, R., Q. Zeng, Z. Ji and D. Gun (1992): Numerical simulation for a northeastward flowing current from area off the eastern Hainan Island to Tsugaru/Soya Strait. *La Mer*, **30**, 229–238.

Lozano, C. J., A. R. Robinson, H. G. Arango, A. Gangopadhyay, Q. Sloan, P. J. Haley, L. Anderson and W. Leslie (1996): An interdisciplinary ocean prediction system: assimilation strategies and structure data model. p. 413–452. In *Modern Approaches to Data Assimilation in Ocean Modeling*, ed. by P. Malanotte-Rizzoli, Elsevier, Amsterdam.

Metzger, E. J. and H. E. Hurlburt (1996): Coupled dynamics of the South China Sea, the Sulu Sea, and the Pacific Ocean. *J. Geophys. Res*., **101**, 12,331–12,352.

Nitani, H. (1970): Oceanographic conditions in the sea east of Philippines and Luzon Strait in summer of 1965 and 1966. p. 213–232. In *The Kuroshio—A Symposium on Japan Current*, ed. by J. D. Marr, East-West Press, Honolulu, Hawaii.

Qiu, D. Z., Y. T. Huang, L. M. Chen and Z. X. Guo (1985): Circulation structures in the studied waters. *Comprehensive Investigations and Studies of the South China Sea*, Vol. 2, Science Press, Beijing, p. 204–230 (in Chinese).

Shaw, P. T. (1989): The intrusion of water masses into the sea southwest of Taiwan. *J. Geophys. Res*., **94**, 18,213–18,226.

Shaw, P. T. (1991): The seasonal variation of the intrusion of the Philippine Sea water into the South China Sea. *J. Geophys. Res*., **96**, 821–827.

Soong, Y. S., J. H. Hu, C. R. Ho and P. P. Niiler (1995): Cold-core eddy detected in South China Sea. *Eos Trans. AGU*, **76**, 345–347.

South China Sea Institute of Oceanology (1985): Integrated Investigation Report on Sea Area of the South China Sea, Vol. 2, p. 183–231, Science Press, Beijing (in Chinese).

Teague, W. J., M. J. Carron and P. J. Hogan (1990): A comparison between the Generalized Digital Environmental Model and Levitus climatology. *J. Geophys. Res*., **95**, 7,167–7,183.

Wu, C. R., P. T. Shaw and S. Y. Chao (1999): Assimilating altimetric data into a South China Sea model. *J. Geophys. Res*., **104**, 29,987–30,005.

Wyrtki, K. (1961): Scientific results of marine investigations of the South China Sea and Gulf of Thailand 1959–1961, Naga Rep., 2, p. 164–169, Scripps Institution of Oceanography, University of California, San Diego.

Xu, X. Z., Z. Qiu and H. C. Chen (1982): The general description of the horizontal circulation in the South China Sea. *Proceedings of the Symposium of the Chinese Society of Marine Hydrology and Meteorology, Chinese Society of Oceanology and Limnology*, Science Press, Beijing, p. 119–127 (in Chinese with English abstract).

Zhou, F. X., J. J. Shen, A. L. Berestov and A. D. Marushkevich (1995): Seasonal features of large-scale geostrophic circulations in the South China Sea. *Tropical Oceanol*., **14**(4), 9–14 (in Chinese with English abstract).